Supporting Information

van der Cruijsen et al. 10.1073/pnas.1305563110

SI Methods

Structural Analysis and Validation. A homology model of KcsA-Kv1.3 in the close conductive state was generated from the tetramer structure of full-length KcsA (1) [Protein Data Bank (PDB) ID code 3EFF] and used to predict CC and CHHC solid-state NMR (ssNMR) spectra. Chemical shift assignments were largely used from previous work (2). Missing assignments were supplemented by SPARTA backbone predictions and average side-chain carbon chemical shifts taken from the Biological Magnetic Resonance Bank. The structural analysis involved CHHC spectra recorded using mixing times of 50 μs, 250 μs, and 500 μs (Fig. S1) in the closed state and 50 μs and 250 μs in the inactivated state (Fig. S5*A*). Data were analyzed with a ^{1}H-^{1}H distance cutoff of 6 Å and a predicted correlation was verified if the signal to noise exceeded a value of 3 in the respective experimental spectrum. Peaks located close to the diagonal of the spectrum or to spinning side bands were manually removed.

Monomer structures for KcsA-Kv1.3 were computed by simulated annealing in Crystallography and NMR System (CNS) software (3) starting from an extended conformer (residues 22–160). Homology-derived ssNMR ^{1}H-^{1}H distance restraints from CHHC spectra along with the unambiguous resolved long- and medium-range contacts identified from [^{2}H,^{13}C,^{15}N] KcsA-Kv1.3 and dihedral angle restraints obtained from PREDITOR (4) using experimental chemical shifts and values estimated from the KcsA structural homologue (PDB ID code 3EFF) were represented by soft-square-well potentials. Dihedral angles for residues 50 to 65 containing the 11 mutations distinguishing KcsA and KcsA-Kv1.3 were exclusively based on experimental chemical shifts. The simulated annealing procedure followed the standard CNS protocol except for an increased number of steps performed during the high temperature (n = 2,000), first slow-cooling (n = 6,000), and second slow-cooling (n = 5,000) annealing stages. We generated 400 structures and selected 15 based on lowest overall energy for further analysis. We observed convergence to a unique structure for the pore domain of KcsA-Kv1.3 (residues 22–115). Structures of the C-terminal residues 116 to 160 diverged, possibly as a result of an insufficient number of assignments and structural constraints. In addition, residues 1 to 20 were used for assignment (ref. 2) and cross validation. The final structural models exhibited backbone RMSDs (for residues 44–90 and given in Angstrom) of 0.3 (KcsA-Kv1.3: closed state), 1.0 (KcsA-Kv1.3: inactivated state) and 0.33 (KcsA: closed state).

The ssNMR structural models were validated by back-predicting CHHC spectra with ^{1}H-^{1}H distances determined with the lowest energy structure for the closed as well as the inactivated state of KcsA-Kv1.3. First, we confirmed that predicted spectra reproduced experimental cross peak positions. In the second stage, we further analyzed those correlations that were based on unambiguous experimental assignments for KcsA-Kv1.3. Within this subset, we identified 15 additional (medium- and long-range) CHHC correlations for the closed state and four additional ones for the inactivation state that are unique and unambiguous for the 3D ssNMR models of KcsA-Kv1.3. Likewise, the final structure significantly improved chemical shift predictions using SPARTA (5) for the turret region compared with the starting structure.

The structural model of WT KcsA was obtained by using a similar strategy. First, the full-length KcsA (1) (PDB ID code 3EFF) structure was used to predict CC and CHHC ssNMR spectra. Resonance assignments for residues that differ from KcsA-Kv1.3 were obtained de novo (Fig. S6*B*). The structural analysis involved CHHC spectra recorded by using mixing times of 250 μs (Fig. S7*A*) and 500 μs. Data were analyzed with a ^{1}H-^{1}H distance cutoff of 6 Å, and a predicted correlation was verified if the signal-to-noise ratio exceeded a value of 3 in the respective experimental spectrum. Peaks located close to the diagonal of the spectrum or to spinning side bands were manually removed. The determination of the monomer structure then proceeded as described with the use of dihedral angle restraints that were updated by the resonance assignments of the mutation site in KcsA (Fig. S6*A*) vs. KcsA-Kv1.3. The simulated annealing procedure followed the standard CNS protocol except for an increased number of steps performed during the high temperature (n = 1,000), first slow-cooling (n = 2,000), and second slow-cooling (n = 5,000) annealing stages.

Tetramer Generation Using Multibody Docking. The KcsA-Kv1.3 tetramer model was calculated by using the multibody docking routine of the HADDOCK Web server (6). First, four identical copies (M1–M4) of the lowest energy monomeric structure for the closed state of KcsA-Kv1.3 (residues 22–115) were obtained by using simulated annealing molecular dynamics (MD) refinement in CNS. These structures were supplied, along with 23 intermonomer contacts identified from the fractional deuteration studies, as input during the docking run. The C4 symmetry of the tetramer was defined by imposing six C2 symmetry pairs between the monomers M1–M2, M2–M3, M3–M4, M4–M1, M1–M3, and M2–M4. Standard settings were used in the HADDOCK-simulated annealing protocol. All models obtained from the simulated annealing refinement subsequently followed the explicit solvent refinement in DMSO as a mimic for a membrane environment. The final structures were ranked on the basis of total energy.

1. Uysal S, et al. (2009) Crystal structure of full-length KcsA in its closed conformation. *Proc Natl Acad Sci USA* 106(16):6644–6649.
2. Schneider R, et al. (2008) Solid-state NMR spectroscopy applied to a chimeric potassium channel in lipid bilayers. *J Am Chem Soc* 130(23):7427–7435.
3. Brünger AT, et al. (1998) Crystallography & NMR system: A new software suite for macromolecular structure determination. *Acta Crystallogr D Biol Crystallogr* 54(pt 5): 905–921.
4. Berjanskii MV, Neal S, Wishart DS (2006) PREDITOR: A Web server for predicting protein torsion angle restraints. *Nucleic Acids Res* 34(Web server issue):W63–W69.
5. Shen Y, Bax A (2007) Protein backbone chemical shifts predicted from searching a database for torsion angle and sequence homology. *J Biomol NMR* 38(4):289–302.
6. de Vries SJ, van Dijk M, Bonvin AM (2010) The HADDOCK Web server for data-driven biomolecular docking. *Nat Protoc* 5(5):883–897.

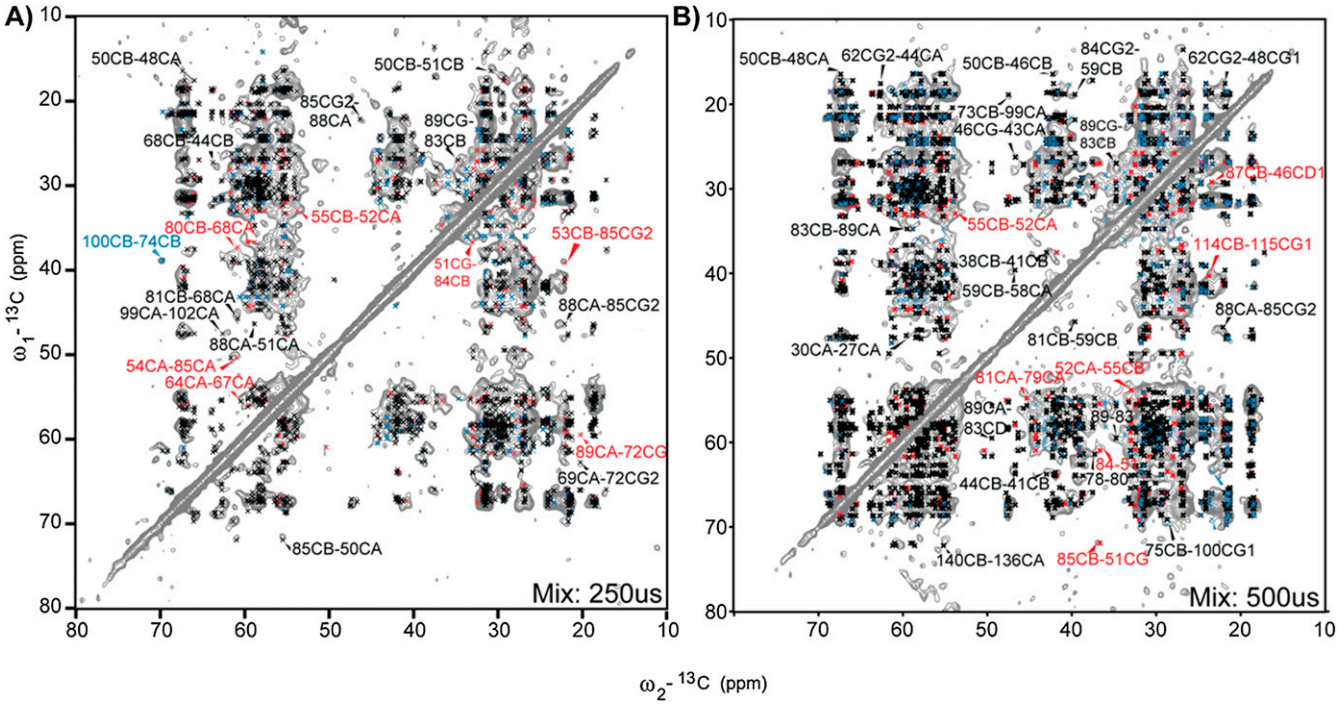

Fig. S1. ssNMR-based hybrid approach to determine 3D structural models of the KcsA-Kv1.3 chimeric channel. CHHC (1) spectrum of the closed state of the KcsA-Kv1.3 using ^{1}H-^{1}H mixing times of 250 μs (*A*) and 500 μs (*B*). Predicted intramolecular (black cross peaks) and intermolecular (blue cross peaks) correlations based on the homology structure (PDB ID code 3EFF) (2) that are in agreement with the experimental data are indicated. Additional unique correlations observed with the generated structure of KcsA-Kv1.3 are shown by red crosses.

1. Lange A, Seidel K, Verdier L, Luca S, Baldus M (2003) Analysis of proton-proton transfer dynamics in rotating solids and their use for 3D structure determination. *J Am Chem Soc* 125(41): 12640–12648.
2. Uysal S, et al. (2009) Crystal structure of full-length KcsA in its closed conformation. *Proc Natl Acad Sci USA* 106(16):6644–6649.

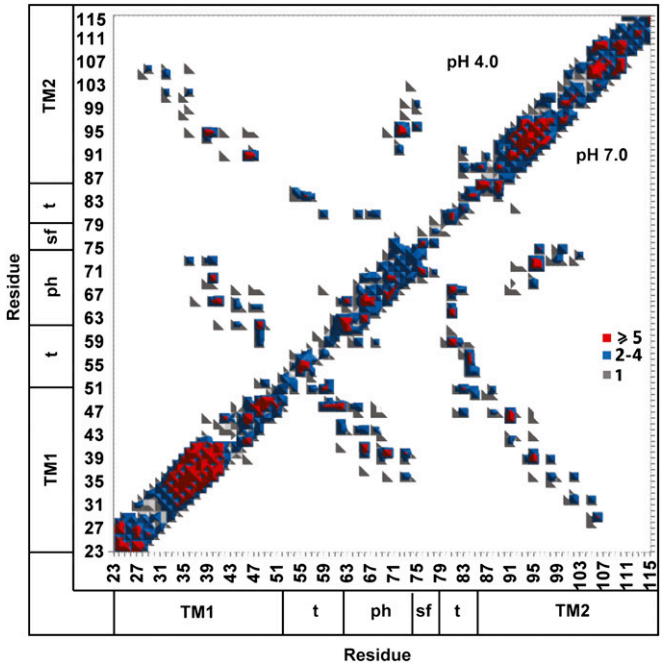

Fig. S2. Correlation matrix indicating structural restraints for KcsA-Kv1.3 before and after inactivation. Data encode distance restraints identified from CHHC (1) data obtained on [U-^{13}C,^{15}N]KcsA-Kv1.3 and CC correlation spectra recorded on [^{2}H,^{13}C,^{15}N]KcsA-Kv1.3 that were used for the structure calculation of the closed (pH 7) and inactivated (pH 4) states of KcsA-Kv1.3.

1. Lange A, Seidel K, Verdier L, Luca S, Baldus M (2003) Analysis of proton-proton transfer dynamics in rotating solids and their use for 3D structure determination. *J Am Chem Soc* 125(41): 12640–12648.

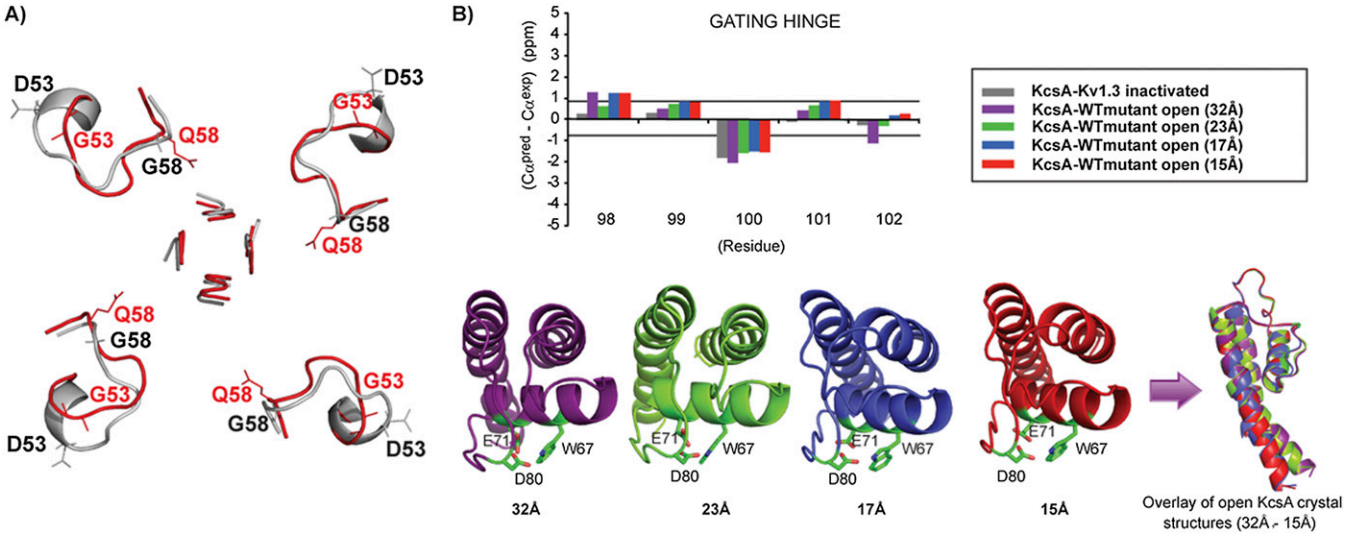

Fig. S3. Structural analysis of KcsA-Kv1.3 before and after inactivation. (*A*) Top view (or surface view) of the superimposed turret regions (residue 52–60) of the ssNMR structure of KcsA-Kv1.3 (gray) and the crystal structure of parent KcsA showing a widening of the pore for the chimeric channel. (*B*) (*Upper*) Differences between predicted and experimental Cα chemical shifts for the inactivated state of KcsA-Kv1.3 and the open KcsA crystal structures for the residues 98 to 102 in the gating hinge region. The horizontal line at 0.98 ppm represents the rms prediction error value for Cα atom for ssNMR data reported earlier (1). (*Lower*) Extracellular view of the four open state crystal structures of mutant KcsA (2) classified based on the Cα–Cα intersubunit distances at Thr-112 residue (*Left*) and overlay of all structures (*Right*). Note that the pore loop region of the truncated KcsA remains unaltered in all structures.

1. Seidel K, Etzkorn M, Schneider R, Ader C, Baldus M (2009) Comparative analysis of NMR chemical shift predictions for proteins in the solid phase. *Solid State Nucl Magn Reson* 35(4):235–242.
2. Cuello LG, Jogini V, Cortes DM, Perozo E (2010) Structural mechanism of C-type inactivation in K(+) channels. *Nature* 466(7303):203–208.

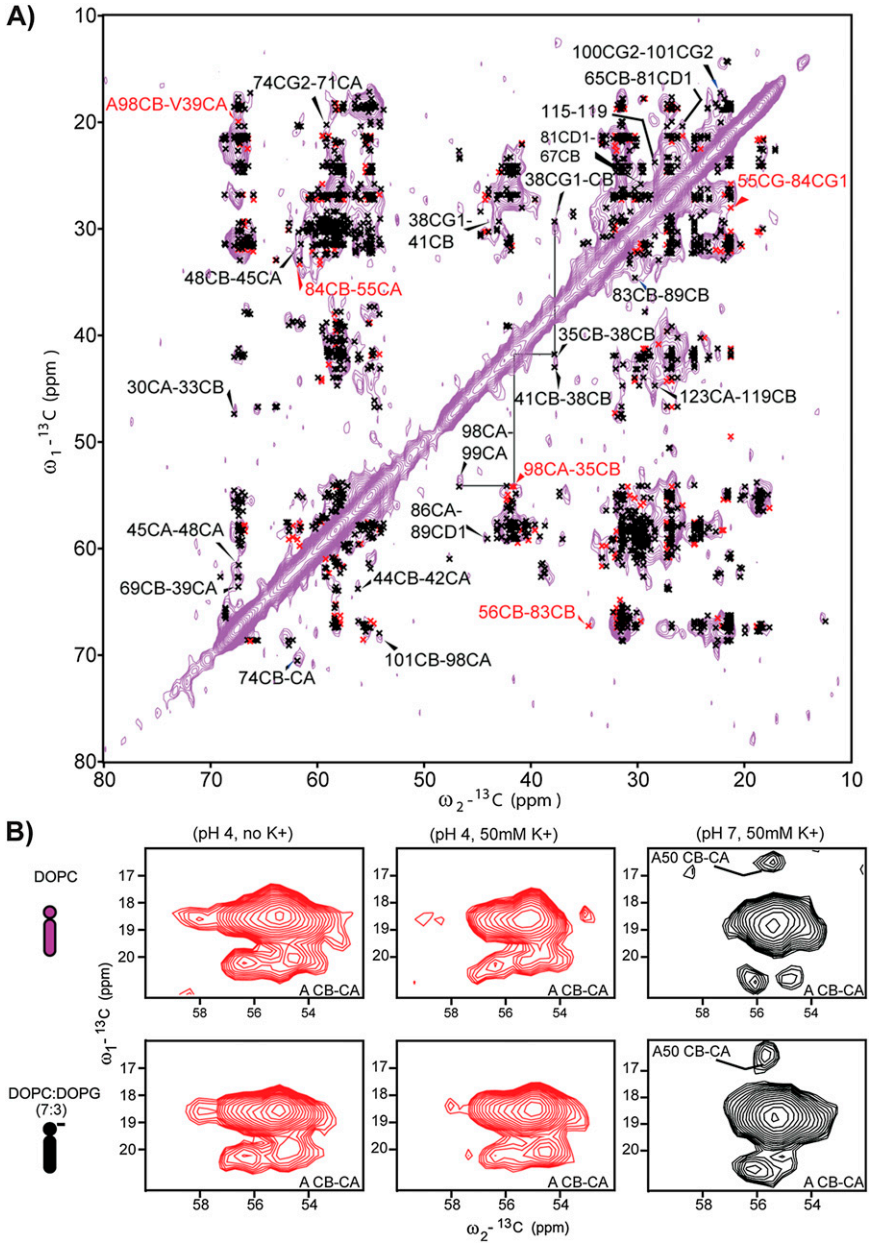

Fig. S4. ssNMR data on KcsA-Kv1.3 after inactivation and after back-titration to pH 7. (*A*) CHHC spectrum using a ^{1}H-^{1}H mixing time of 250 μs on the inactivated state of the KcsA-Kv1.3 channel embedded in asolectin lipid bilayers. Black cross peaks represent predicted correlations based on the initial structure that are in agreement with the experimental data. Red cross peaks represent additional unique correlations observed in the inactivated state. (*B*) Spectral cutouts of (^{13}C,^{13}C) ssNMR experiments in two different lipid bilayer settings that reveal the reoccurrence of the cross peak pattern of the extended α-helix in the TM1T segment after back-titration to pH 7 from 0 and 50 mM K^{+}.

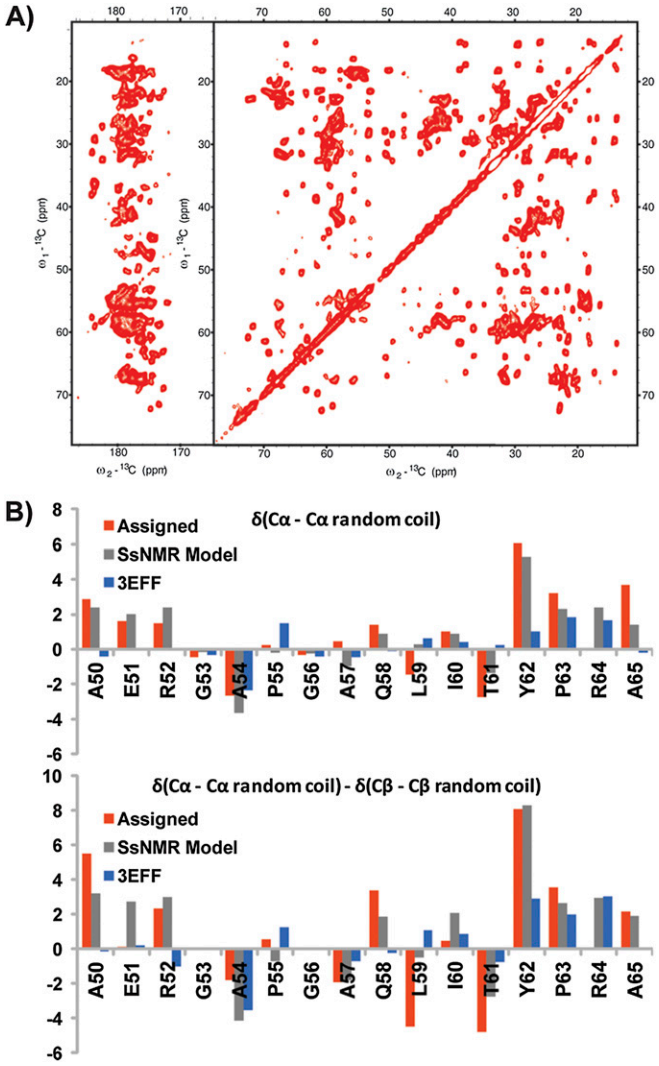

Fig. S5. ssNMR on WT KcsA and resonance assignments of the KcsA turret. (*A*) Two-dimensional ssNMR homonuclear (^{13}C-^{13}C) 30 ms proton-driven spin diffusion spectra of KcsA reconstituted in asolectin, pH 7, with 50 mM K^+ recorded at 700 MHz ^1H Larmor frequency and 11 KHz magic angle spinning. (*B*) Comparison of Cα (*Top*) and Cα-Cβ (*Bottom*) secondary chemical shifts with reference to random coil values taken from Wang et al. (1). Positive values indicate helical conformation. Note that predictions based on ssNMR structural model are in better agreement than predictions using the X-ray structure (PDB ID code 3EFF).

1. Wang Y, Jardetzky O (2002) Probability-based protein secondary structure identification using combined NMR chemical-shift data. *Protein Sci* 11(4):852–861.

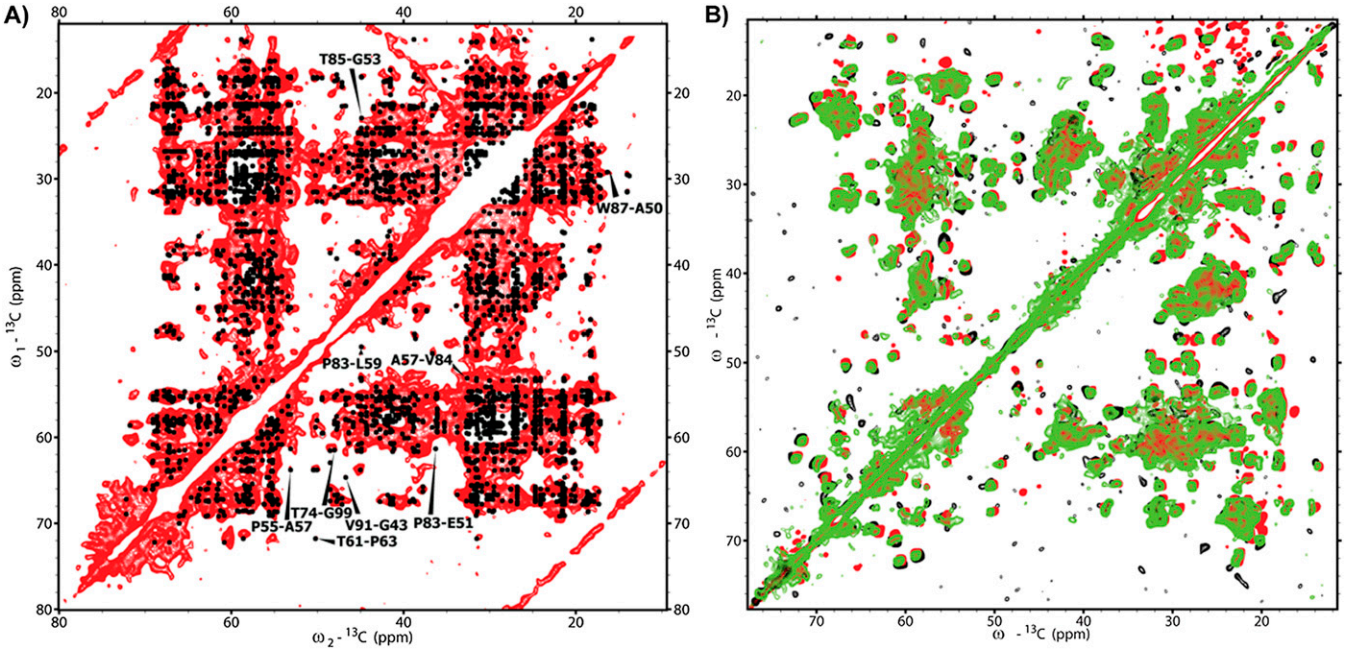

Fig. S6. CHHC KcsA and CC KcsA E71 mutant ssNMR spectra. (*A*) CHHC spectrum recorded with a ^{1}H-^{1}H mixing time of 250 μs for uniformly (^{13}C,^{15}N) labeled KcsA in the closed conductive state and embedded in asolectin lipid bilayers. Black crosses represent predicted correlations based on the ssNMR 3D structural model of KcsA, which are in agreement with the experimental data. Assigned peaks are visible in Fig. 3*A*. (*B*) 2D (^{13}C,^{13}C) Correlation spectra obtained for KcsA (red) and KcsA-OM-E71Q and -E71A (green and black, respectively) at pH 7.4, 50 mM [K^+] reconstituted in asolectin.

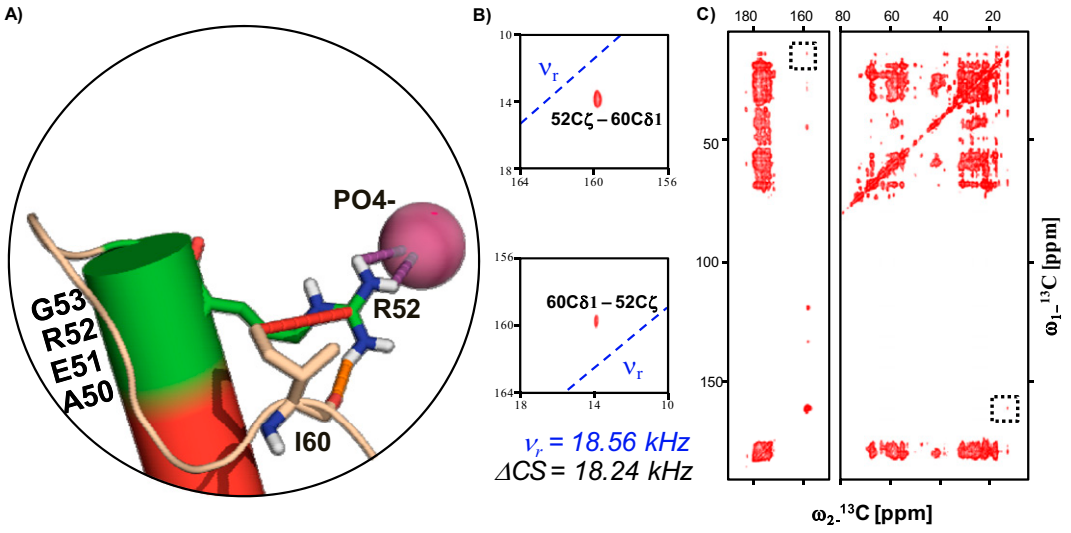

Fig. S7. Combined MD–ssNMR analysis. (*A*) MD simulations suggest that the helical elongation of TM1 until residue G53 in WT KcsA is stabilized by an intramolecular hydrogen bond (orange line) between R52 and I60, which is in turn stabilized by the presence of the membrane (magenta lines; Figs. 4*A* and 5). The spatial proximity of these two residues was experimentally verified (red line) by (*B* and *C*) 2D ^{13}C-^{13}C rotational resonance experiment by matching the spinning frequency ω_r to the chemical shift difference between R52Cζ and I60 δ1. (*C*) No decoupling was applied during the mixing time of 200 ms to broaden the matching condition. Note that the contact R52Cζ and I60 δ1 is unambiguous, as the I60 side-chain CH_3 carbons feature well-resolved chemical shifts, and R52 is the only arginine on KcsA's extracellular side.

Table S1. Structural restraint statistics for KcsA-Kv1.3 in closed and inactivated state

Restraints	Number of constraints
KcsA-Kv1.3 (closed state, pH 7.0)	
Distance restraints	
^{1}H-^{1}H restraints [CHHC on (U-^{13}C/^{15}N) KcsA-Kv1.3]	
Intraresidue	475 (141)
Sequential ($\|i - j\| = 1$)	569 (148)
Medium-range ($\|i - j\| \leq 4$)	826 (169)
Long-range ($\|i - j\| \geq 5$)	338 (156)
^{13}C-^{13}C restraints [^{13}C-^{13}C PDSD on (^{2}H,^{13}C,^{15}N) KcsA-Kv1.3]	
Medium-range ($\|i - j\| \leq 4$)	42
Long-range ($\|i - j\| > 5$)	36
Total	2,286
Dihedral angle restraints	274
KcsA-Kv1.3 (inactivated state, pH 4.0)	
Distance restraints	
^{1}H-^{1}H restraints [CHHC on (U-^{13}C/^{15}N) KcsA-Kv1.3]	
Intraresidue	440 (135)
Sequential ($\|i - j\| = 1$)	390 (132)
Medium-range ($\|i - j\| \leq 4$))	588 (125)
Long-range ($\|i - j\| \geq 5$)	203 (126)
Total	1,621
Dihedral angle restraints	262

Numbers in parentheses relate to constraints for residues 44–90. PDSD, proton-driven spin diffusion.

Table S2. Structural restraint statistics for KcsA in the closed state

Restraints	Number of constraints
KcsA (closed state, pH 7.0)	
^{1}H-^{1}H restraints [CHHC on (U-^{3}C/^{15}N) KcsA]	
Intraresidue	486 (169)
Sequential ($\|i - j\| = 1$)	635 (210)
Medium-range ($\|i - j\| \leq 4$)	930 (212)
Long-range ($\|i - j\| \geq 5$)	717 (262)
Total	2,768
Dihedral angle restraints	247

Numbers in parentheses relate to constraints for residues 44–90.

Table S3. Activation and deactivation properties of WT and mutant Kv1.3 channels

Channel	$V_{1/2}$, mV	Z	Time rise to peak, ms	τ_{deact}, ms	Experiments
Kv1.3	−24.0 ± 0.6	3.61 ± 0.08	24.8 ± 0.6	26.8 ± 2.5	6
Kv1.3G377A	−22.1 ± 0.8	3.46 ± 0.03	25.5 ± 0.9	19.3 ± 0.6	5
Kv1.3G377V	−23.2 ± 0.9	3.58 ± 0.08	28.2 ± 0.9	20.2 ± 0.8	5
Kv1.3G377F	−22.0 ± 0.9	3.68 ± 0.04	28.6 ± 1.5	17.6 ± 1.7	5

Kv1.3 WT and mutant channels were expressed in *Xenopus* oocytes as previously described (1). Kv1.3 currents were elicited from a holding potential of −80 mV to various test potentials in 10-mV increments. Voltage of $V_{1/2}$ was determined by fitting a Boltzmann equation to the data to the tail currents obtained after repolarization to −100 mV. Z corresponds to the slope of the conductance–voltage relation at $V_{1/2}$. Time rise to peak was measured at +20 mV and corresponds to the time rise of 10–90% current amplitude. Deactivation time course was measured by fitting a single time constant to the tail current. Errors are given as SEM. $V_{1/2}$, half-maximal activation.

1. Ader C, et al. (2009) Coupling of activation and inactivation gate in a K+-channel: Potassium and ligand sensitivity. *EMBO J* 28(18):2825–2834.